Shear Performance Analysis of CLT–Steel Hybrid Joints: Effects of Fastener Geometry and FRP Reinforcement

Seung-Youp Baek,[a] Soon-Il Hong,[b] and Yo-jin Song [b,*]

Cross-laminated timber (CLT) slabs and steel beams can be combined to form hybrid floor systems for long spans and heavy loads. The performance of these systems depends greatly on the shear connections between the CLT slabs and steel beams. In this study, push-out tests were conducted on CLT–steel joints connected with bolts or lag screws. The tests followed the loading procedure specified in EN 26891. Six specimen types were prepared by varying the fastener type, lag screw diameter and length, and reinforcement condition. Carbon fiber reinforced polymer (CFRP) plates were fabricated by laminating pultruded CFRP sheets with epoxy resin, whereas GF plates were fabricated by bonding woven glass-fiber cloth layers with phenol–resorcinol–formaldehyde adhesive. Both types of plates were bonded to the CLT with epoxy resin. CFRP reinforcement increased the strength and stiffness of the joints but resulted in brittle screw fracture. GF reinforcement produced smaller strength gains but showed a more gradual post-peak response. A modified Ramberg–Osgood model was used to describe the nonlinear load–slip behavior. The analytical curves agreed well with the test results ($R^2 > 0.99$). The model parameters reflected differences in fastener geometry and reinforcement condition. The results provide useful data for the design and numerical analysis of CLT–steel composite floor systems.

DOI: 10.15376/biores.21.4.10835-10852

Keywords: Cross-laminated timber (CLT); Timber-steel hybrid joints; Composite floor system; Push-out test; Shear connection; Ramberg–Osgood model; Fiber-reinforced plastic (FRP) reinforcement

*Contact information: a: Department of Building and Urban Research, Korea Institute of Civil Engineering and Building Technology (KICT), 283 Goyang-daero, Ilsanseo-gu, Goyang-si, Gyeonggi-do 10223, Republic of Korea; b: Department of Forest Biomaterials Engineering, College of Forest and Environmental Sciences, Kangwon National University, 1 Kangwondaehak-gil, Chuncheon-si, Gangwon-do 24341, Republic of Korea; *Corresponding author: songyj@kangwon.ac.kr*

INTRODUCTION

With increasing interest in carbon-neutral construction, the building sector requires structural materials that are both sustainable and lightweight. Within this trend, cross-laminated timber (CLT), as a renewable resource, offers various advantages such as low weight, excellent specific strength, dimensional stability, seismic resilience, and favorable fire performance (Brandner *et al*. 2016; Ramage *et al*. 2017). In addition, off-site construction with CLT contributes to shortened construction time, improved quality, and reduced labor demand (Younis and Dodoo 2022). As a result, CLT has gained significant attention as an alternative or complementary material to concrete and steel in mid- to high-rise buildings, large-span structures, and modular systems. However, timber-only CLT floor systems generally have lower flexural stiffness than concrete or steel floor systems, which limits their application in tall buildings or structures requiring high stiffness and ductility (Yin 2018; Bahrami *et al.* 2021). Increasing slab thickness is a straightforward solution, but this approach is structurally and economically inefficient. Therefore, hybrid floor systems have been developed by combining lightweight CLT slabs with steel beams having high flexural stiffness and strength. These systems can be used for long-span floors and efficient load distribution. (Loss and Frangi 2017; Moritani and Martins 2021; Aloisio *et al.* 2024; Azanaw 2025; Yang *et al.* 2025). Indeed, Ataei *et al.* (2019) experimentally validated the flexural performance of steel beam-to-column joints incorporating CLT slabs, demonstrating the potential of CLT–steel hybrid systems as practical solutions for tall buildings.

The structural performance of CLT–steel hybrid floors depends greatly on the behavior of shear connections. Such connections are typically composed of bolts, lag screws, and adhesives (Ataei *et al.* 2019). The type and geometry of fasteners directly affect initial stiffness, ultimate shear strength, slip behavior, failure mode, and even long-term performance, including creep and mechano-sorptive deformations (Chiniforush *et al.* 2019; Zhang and Ling 2022; He *et al.* 2024). Previous studies have primarily focused on evaluating the shear performance of different connector types. For instance, Loss *et al.* (2016a,b) assessed various connection systems through push-out tests and confirmed that inclined screws combined with epoxy resin improved initial stiffness and load capacity. Hassanieh *et al*. (2016) applied the Ramberg–Osgood model to bolts, screws, and grouted-in bolt connections to quantify the load–slip response, demonstrating its applicability to design. They further reported that when fasteners were combined with adhesives, the initial stiffness increased but brittle failure occurred more readily (Hassanieh *et al.* 2017). Aspila *et al.* (2022) proposed a linear elastic analysis method for CLT–steel composite floors to support design-oriented numerical modeling. Owolabi and Loss (2022) quantitatively investigated the flexural behavior of CLT–steel modules through experiments and finite element analysis, confirming their applicability to design. However, few studies have systematically compared geometric variations within the same connector type. The effects of fiber reinforcement on the strength and ductility of CLT–steel connections also require further investigation. Fiber-reinforced polymers such as carbon fiber-reinforced plastic (CFRP) and glass fiber (GF) have been widely used in strengthening timber and concrete elements due to their high tensile strength, lightweight properties, corrosion resistance, and ease of installation. They are also recognized for their ability to mitigate localized brittle failures and improve deformation capacity (Song *et al.* 2019(a); Vahedian *et al.* 2019). Recent studies have further shown that GFRP reinforcement can enhance the bending strength and stiffness of CLT members, while also reducing the sudden brittle load drop observed in unreinforced panels and promoting a more ductile response (Rostampour-Haftkhani *et al*. 2025). Several studies have confirmed the effectiveness of FRP in enhancing the flexural performance of CLT and composite slabs (Song and Hong 2018; Song *et al.* 2022; Baek *et al.* 2025). In addition, FRP reinforcement has been shown to improve the shear resistance of CLT walls (Song *et al.* 2019b; Jung *et al.* 2020), while FRP-laminated timber portal frames demonstrated enhanced ductility under cyclic lateral loading (Song *et al.* 2024). However, most of these achievements have been reported in the context of members (beams, slabs) or frame joints, whereas direct investigations on CLT–steel shear connections remain scarce. Therefore, it is necessary to clarify how FRP reinforcement influences the stiffness, strength, and ductility of CLT–steel joints.

Therefore, in this study, six types of push-out specimens were fabricated to evaluate the structural performance of CLT–steel joints, considering fastener type (bolt and lag screw), the diameter and length of lag screws, and reinforcement of the CLT tension zone with CFRP or GF. The failure modes and load–slip behavior were then analyzed. In addition, a modified Ramberg–Osgood model was employed to numerically characterize the nonlinear behavior of the joints. The results were used to examine the effects of fastener geometry and FRP reinforcement on the joint performance.

EXPERIMENTAL

Material Properties

Cross-laminated timber (CLT)

The CLT specimens used in this study were fabricated from kiln-dried laminae of Japanese larch (Larix kaempferi (Lamb.) Carr.). Each lamina had a cross-sectional dimension of 120 mm in width and 30 mm in thickness. Five layers were laminated to form CLT panels with final dimensions of 450 mm × 360 mm × 150 mm. The average air-dry moisture content (M.C.) of the fabricated CLT was 12.0 ± 0.2%, and the average air-dry density (ρ) was measured as 599.2 ± 4.5 kg/m³. According to the Korean Standard KS F 2081, the strength grade of the laminae was classified as C–E12–10, which corresponds to a design modulus of elasticity of 12 GPa in the longitudinal direction and 10 GPa in the transverse direction. The reference bending properties for this grade are a modulus of elasticity (E) of 9.6 GPa and a bending strength (f_b) of 28.6 MPa. Phenol–resorcinol–formaldehyde (PRF) adhesive was used to bond the laminae. The detailed dimensions and mechanical properties of the CLT are summarized in Table 1.

Table 1. Dimensions and Mechanical Properties of CLT

Timber type	Grade	Size t × w × l (mm)	M.C. (%)	ρ (kg/m^3)	f_b (MPa)	E (GPa)
CLT	C-E12-E10	450 × 360 × 150	12 ± 0.5	599.2 ± 4.5	28.6	9.6

Steel profile

The beam element connected to the CLT was a hot-rolled I-section steel profile manufactured in accordance with the KS D 3502 standard. The section dimensions were 300 mm in depth and 150 mm in flange width. The nominal yield strength (f_y) and ultimate tensile strength (f_u) of the steel were specified as 275 MPa and 510 MPa, respectively. The cross-sectional dimensions and mechanical properties of the steel profile are summarized in Table 2.

Table 2. Dimensions and Mechanical Properties of Steel Profiles

Type	Section depth d (mm)	Flange width b_f (mm)	Flange thickness t_f (mm)	Web thickness t_w (mm)	Yield strength f_y (MPa)	Ultimate strength f_u (MPa)
Steel profile	300	150	8	8	275	510

Fasteners

Two types of mechanical fasteners were used in the CLT–steel joints. The first was a high-strength bolt with diameter 12 mm and length 150 mm. It was used as the reference connection. The second was a lag screw, applied in three configurations to investigate the effects of fastener geometry: Ø10 × 125 mm, Ø12 × 100 mm, and Ø12 × 125 mm.

Specimen details

In the intended floor system, the CLT slab is placed horizontally above the steel beam, and the mechanical fasteners transfer longitudinal shear at the CLT–steel interface. For the push-out tests, a symmetric CLT–steel–CLT configuration was adopted to reproduce the shear transfer at the interfaces while minimizing load eccentricity. Therefore, the CLT slabs were oriented vertically during testing, unlike their horizontal orientation in the actual floor system. To evaluate the shear performance of CLT–steel joints, a total of six types of push-out specimens were fabricated (Fig. 1). All specimens consisted of a symmetric CLT–steel–CLT configuration, in which two fasteners were installed on each side of a single steel profile. The end distance (measured from the edge of the outermost lamina of the CLT) was fixed at 100 mm, and the spacing between fasteners was 80 mm for all specimens. Specimens were categorized into three groups: bolted joints, lag screw joints, and reinforced lag screw joints. The B-12-150 specimen used high-strength bolts with diameter 12 mm and length 150 mm. A 13 mm through-hole was drilled in the CLT. The bolt was directly fastened to the steel profile. The lag screw joints were fabricated with three geometries to investigate the effects of screw diameter and embedment depth: Ø10 × 125 mm (LS-10-125, embedment depth = 9.5d), Ø12 × 100 mm (LS-12-100, embedment depth = 7.5d), and Ø12 × 125 mm (LS-12-125, embedment depth = 9.5d).

For the reinforced joints, specimen CRLS-12-100 used lag screws with Ø12 × 100 mm (embedment depth 7.5d), while the outermost tensile lamina of the CLT in contact with the steel profile was replaced with a CFRP laminate plate (15 mm thick, 120 mm wide). The CFRP plate was fabricated by laminating ten 1.5 mm-thick pultruded CFRP sheets with epoxy resin. Each sheet consisted of carbon fibers embedded in an epoxy resin matrix, and the fabricated plate was bonded to the CLT using epoxy resin. Specimen GRLS-12-100 also used Ø12 × 100 mm lag screws (embedment depth 7.5d), but the outer surface of the CLT tensile lamina was reinforced with GF cloth. The GF plate was fabricated by laminating five 0.5 mm-thick woven glass-fiber cloth layers with PRF adhesive, resulting in a final thickness of 2.5 mm and a width of 150 mm. The fabricated GF plate was bonded to the CLT using epoxy resin. The specimen designation rule is as follows: the first symbol indicates the fastener type (B: bolt; LS: lag screw; CRLS: CFRP-reinforced lag screw; GRLS: GF-reinforced lag screw), the second number denotes the fastener diameter (mm), and the third number denotes the fastener length (mm). The detailed specifications of each specimen are given in Table 3.

Table 3. Details and Reinforcement Conditions of Push-out Test Specimens

Specimens	Shear connector		Embedment depth	Reinforcement (Size: *T* × *W* (mm))	Repeats
	Type	Size: *d* × *l* (mm)			
B-12-150	High-strength bolt	12 × 150	Full penetration (CLT through-hole Ø13 mm)	None	4
LS-10-125	Lag screw	10 × 125	9.5d	None	4
LS-12-125	Lag screw	12 × 125	9.5d	None	4
LS-12-100	Lag screw	12 × 100	7.5d	None	4
CRLS-12-100	Lag screw	12 × 100	7.5d	CFRP plate (15 × 120)	4
GRLS-12-100	Lag screw	12 × 100	7.5d	GF cloth (2.5 × 150)	4

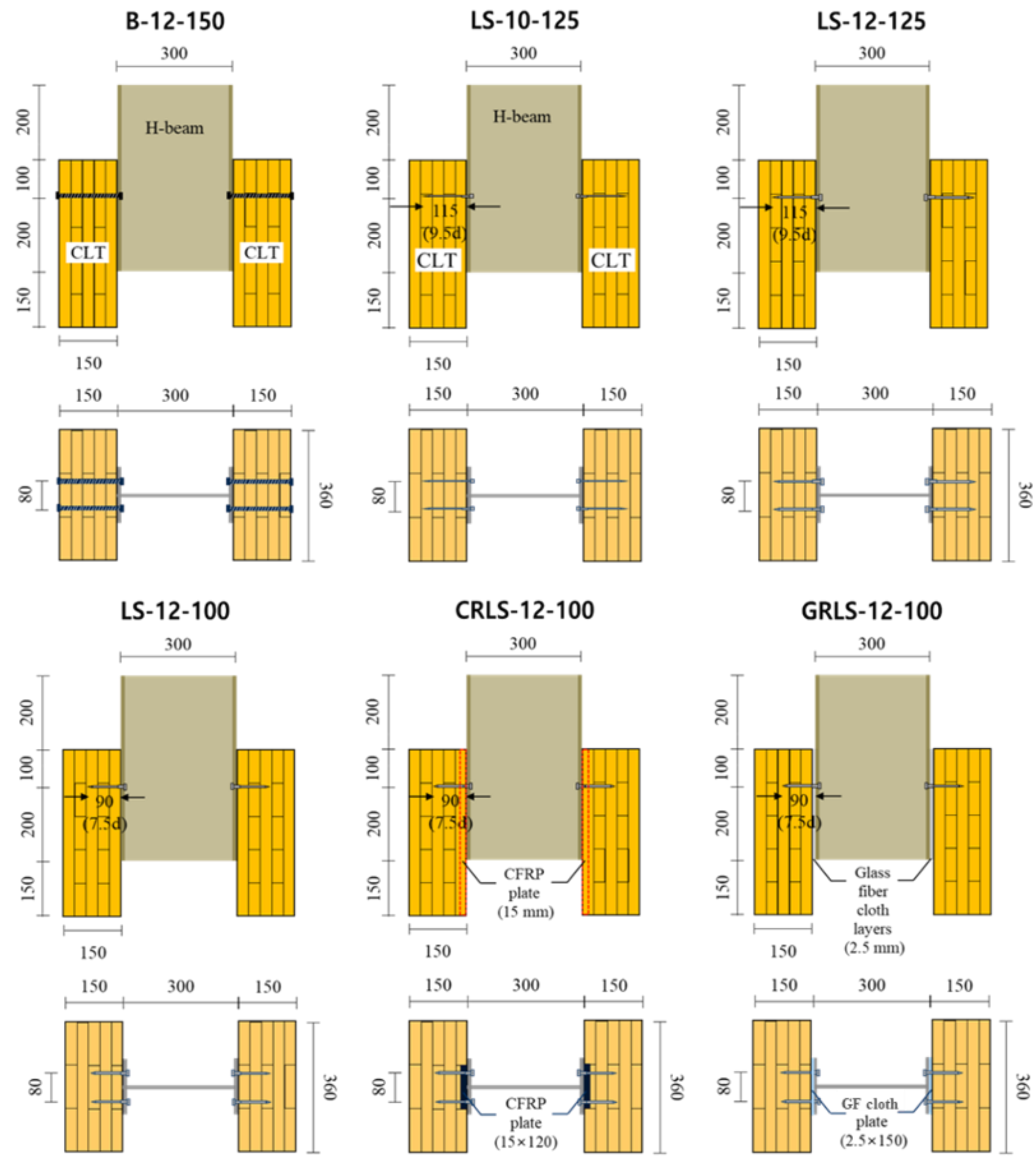

Fig. 1. Types and configurations of push-out test specimens (all dimensions in mm)

Instrumentation and Loading Procedure

The shear performance of the CLT–steel joints was evaluated through push-out tests using a vertical loading machine with a maximum capacity of 300 kN. As illustrated in Fig. 2, the load was applied to the cross-section of the steel profile, aligned parallel to the longitudinal axis of the steel member. To measure slip, two displacement transducers were installed on both the front and rear sides of the joint at the same height as the fastener locations, enabling precise measurement of the relative displacement between the CLT slab and the steel profile.

The loading protocol followed the procedure specified in EN 26891 (1991) and was carried out in two stages (Fig. 3). In the first stage, the load was gradually increased to 40% of the estimated ultimate load within 120 seconds and then maintained for 30 seconds. The load was subsequently reduced to 10% of the estimated ultimate load and held constant for another 30 seconds. In the second stage, the load was continuously increased until failure occurred. The estimated ultimate load for each specimen type was determined from preliminary tests.

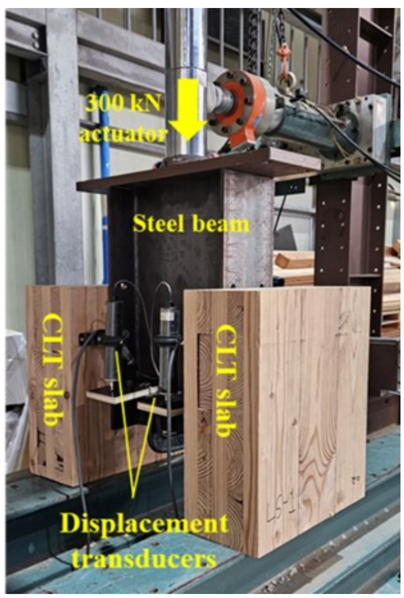

Fig. 2. Push-out test setup for CLT–steel joint

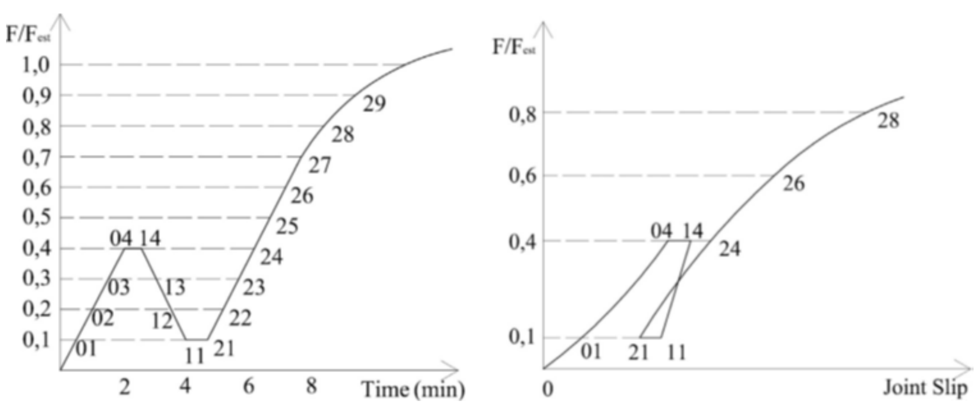

Fig. 3. Loading protocol for the push-out test (BS EN 26891 1991)

RESULTS AND DISCUSSION

Failure Modes

Fasteners in the CLT–steel joints were subjected to single shear loading. Their failure behavior varied depending on fastener type, geometry, strength, and reinforcement condition. The observed failure mechanisms were categorized into four distinct modes. Failure Mode I corresponds to bearing failure occurring in the surrounding CLT without noticeable plastic deformation of the fastener. Failure Mode II is characterized by the formation of a single plastic hinge in the fastener, whereas Failure Mode III involves the development of two plastic hinges. Failure Mode IV refers to fracture of the fastener itself. In general, Modes I and IV in timber–steel joints are classified as brittle failures, while Modes II and III represent ductile or semi-ductile behaviors (Hassanieh *et al.* 2016).

Bolt-type connection (B-12-150)

For the B-12-150 specimen, in which the CLT and steel profile were connected with high-strength bolts. Two plastic hinges were typically formed in the bolt at the shank and threaded regions, corresponding to Failure Mode III, while in some cases fracture of the threaded portion occurred, corresponding to Mode IV (Fig. 4(a)). In addition, bearing failure caused by the fasteners was also observed in the CLT tension zone in contact with the steel profile. The bolted joints showed both semi-ductile behavior associated with Mode III and brittle fracture associated with Mode IV.

Lag screw connections without reinforcement (LS-10-125, LS-12-125, LS-12-100)

For lag screw joints, specimen LS-10-125 primarily exhibited Mode IV (screw fracture) (Fig. 4(b)), whereas specimens LS-12-125 and LS-12-100 showed a mixture of Mode III (two plastic hinges) and Mode IV (Fig. 4(c)). This difference was closely related to the length-to-diameter ratio (L/d) of the fasteners. The calculated L/d ratios were 12.5 for LS-10-125, 10.4 for LS-12-125, and 8.3 for LS-12-100. As the L/d ratio decreased, the screws tended to develop two plastic hinges. Moreover, the locations of the plastic hinges in LS-12-125 and LS-12-100 varied depending on screw length, suggesting that embedment depth and restraint conditions influenced hinge formation. Similar to the bolted joints, bearing failure of the CLT tensile lamina was observed in all lag screw specimens.

Reinforced lag screw connections (CRLS-12-100, GRLS-12-100)

For the reinforced joints, specimen CRLS-12-100 with a CFRP plate predominantly failed in Mode IV (screw fracture), while some screws also exhibited Mode II (single plastic hinge) (Fig. 4(d)). The CFRP reinforcement layer effectively suppressed bearing failure in the CLT tension zone; however, as a result, stress was concentrated on the fasteners, and brittle fracture was observed in most screws. This indicates that stiffness mismatch between timber and CFRP resulted in load concentration on the fastener.

In contrast, specimen GRLS-12-100, reinforced with GF cloth, exhibited a combination of Modes III and IV, accompanied by bearing failure in the CLT tensile lamina, similar to the unreinforced joints (Fig. 4(e)). GF reinforcement did not markedly change the failure mode, but it reduced local CLT damage and produced a gradual post-peak response.

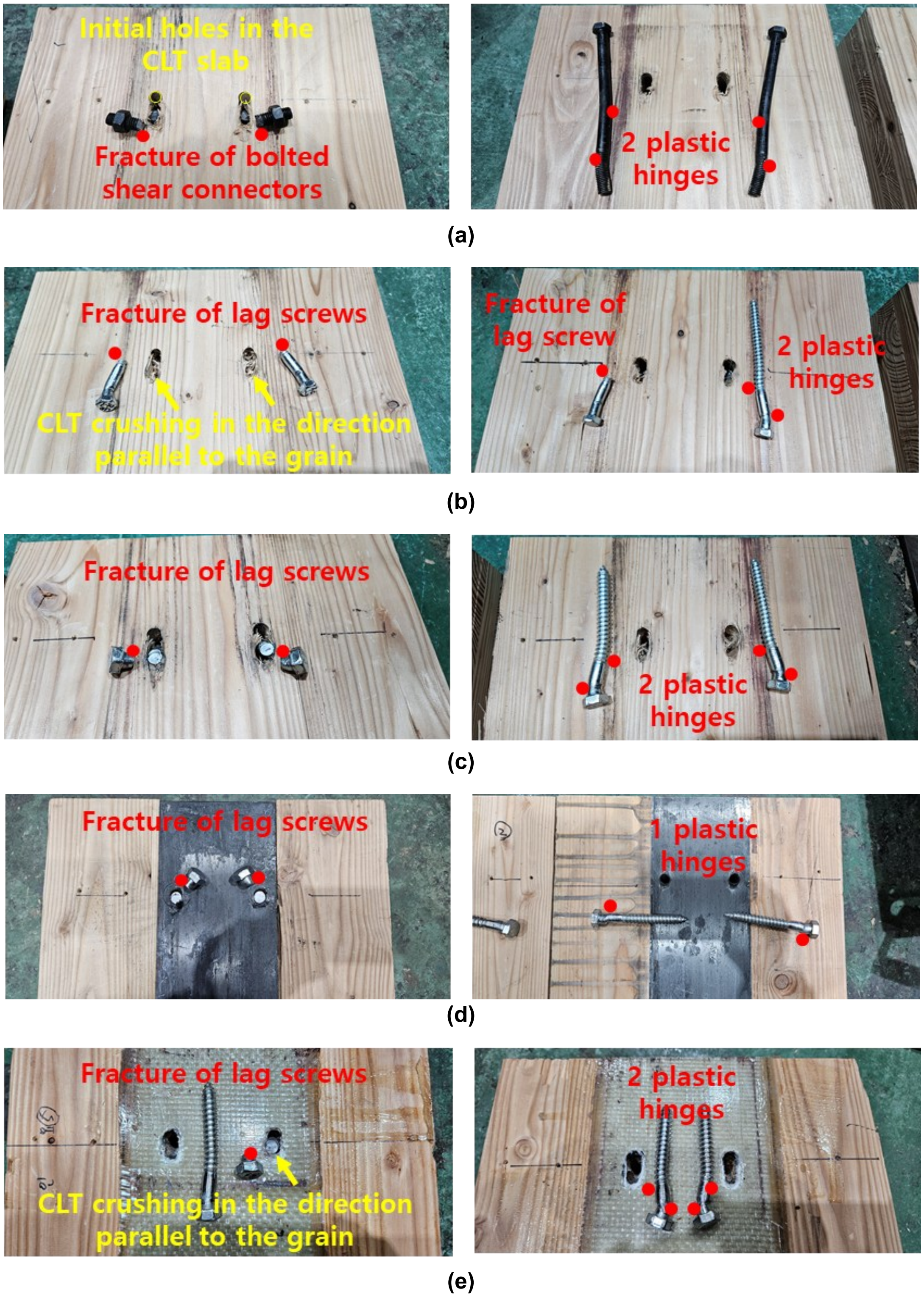

Fig. 4. Failure modes of (a) B-12-150, (b) LS-10-125, (c) LS-12-125 and LS-12-100, (d) CRLS-12-100, (e) GRLS-12-100

Load-Slip Behavior

The load–slip curves of the CLT–steel hybrid joints obtained from the push-out tests are shown in Fig. 5, and the main strength properties derived from them are summarized in Table 4. Slip values were calculated as the average of the displacement transducer readings installed on each specimen. In addition, Table 5 summarizes the structural responses for each joint type, including the main failure mode, fastener type and reinforcement condition, plastic deformation characteristics, screw fracture, and level of ductility.

Bolt-type connection

Specimen B-12-150, connected with high-strength bolts (Fig. 5(a)), exhibited the highest initial shear stiffness ($k_{s,0.4}$ = 147.7 kN/mm) and ultimate load ($F_{\max}$ = 191.9 kN) among all joints, owing to the post-tensioning effect of the bolts. The load–slip curves showed some variation in initial stiffness, whereas the maximum loads were relatively consistent (COV: $k_{s,0.4}$ = 66.3%, F_{max} = 3.7%). The ductility index (μ) was 8.7, demonstrating a wide plastic range and large slip capacity prior to reaching the maximum load, which is advantageous for energy absorption and ductility. However, a sharp drop in load-carrying capacity was observed after peak load, indicating an overall brittle behavior.

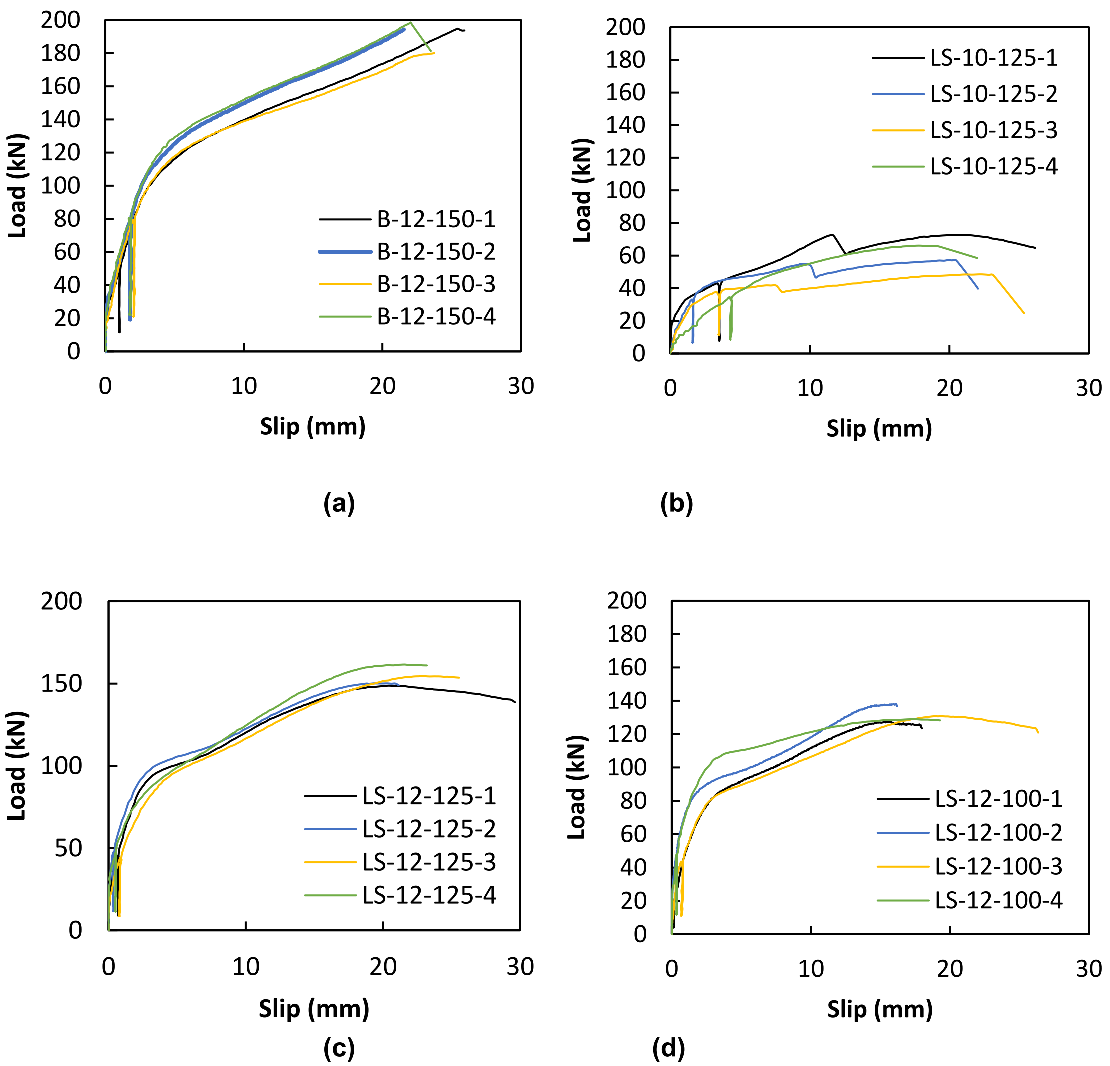

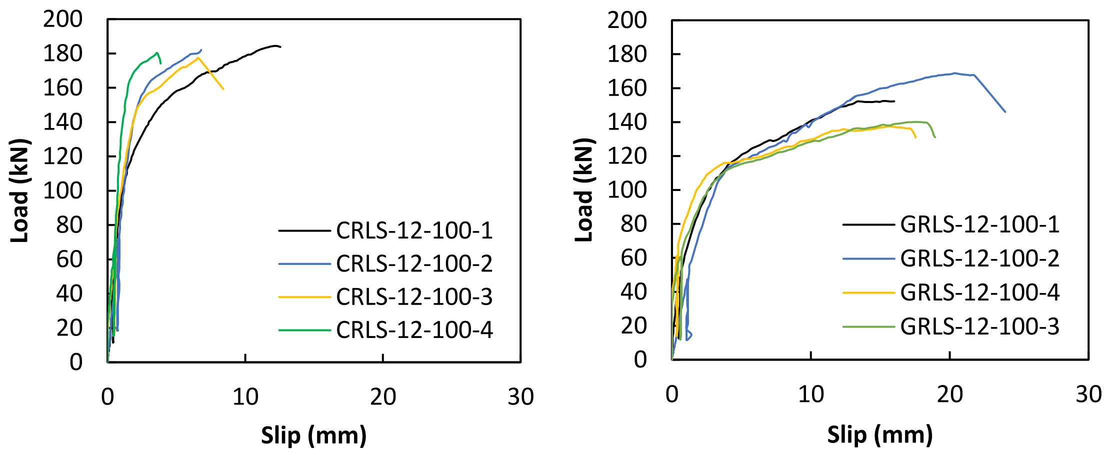

(e) (f)

Fig. 5. Load-slip curves of (a) B-12-150, (b) LS-10-125, (c) LS-12-125, (d) LS-12-100, (e) CRLS-12-100, (f) GRLS-12-100

Lag screw connections without reinforcement

Specimen LS-10-125, connected with 10 mm-diameter lag screws (Fig. 5(b)), showed the lowest maximum load (F_{max} = 61.2 kN). Its initial slip modulus, $k_{s,0.4}$, was 119.1 kN/mm, but large variations were observed among the specimens. In most specimens, premature screw fractures occurred irregularly before reaching the maximum load, resulting in large variability among specimens (COV: $k_{s,0.6}$ = 65.3%, F_{max} = 14.9%, μ = 25.4%). Under the tested conditions, the 10 mm screws showed lower strength and less consistent behavior than the 12 mm screws.

Specimens LS-12-125 and LS-12-100, connected with 12 mm-diameter lag screws (Fig. 5(c), (d)), showed enhanced frictional resistance within the joints due to the tightening effect, which suppressed initial slip and improved shear stiffness. Although LS-12-100 recorded an ultimate load (F_{max}) about 14.5% lower than LS-12-125, their yield loads ($F_{y,5\%}$) were similar, and the stiffness values ($k_{s,0.4}$ and $k_{s,0.6}$) of LS-12-100 were 154.8% and 60.0% higher, respectively. These results indicate that increasing fastener length and embedment depth contributes to improving maximum load and response consistency (COV: F_{max} = 7.8%, μ = 10.4%), but may be disadvantageous for initial stiffness. Both joints exhibited gradual softening behavior after the peak load, which is considered beneficial for energy absorption and ductility.

Table 4. Push-out Test Results for CLT-Steel Hybrid Connections

Specimens	F_{max} (kN)	v_{max} (mm)	$F_{y,5\%}$ (kN)	$v_{y,5\%}$ (mm)	$k_{s,0.4}$ (kN/mm)	$k_{s,0.6}$(kN/mm)	μ
B-12-150	191.9 (3.7)	23.2	96.4 (2.0)	2.7	147.7 (66.3)	10.4 (25.1)	8.7 (2.3)
LS-10-125	61.2 (14.9)	20.1	41.5 (7.1)	4.2	119.1 (36.0)	21.1 (65.3)	5.0 (25.4)
LS-12-125	153.7 (3.3)	21.1	75.2 (2.6)	1.9	22.6 (31.2)	7.5 (30.3)	11.5 (12.5)
LS-12-100	131.4 (3.0)	17.2	72.7 (5.1)	1.6	57.6 (67.6)	12.0 (36.0)	11.9 (25.9)
CRLS-12-100	181.0 (1.4)	7.3	128.9 (12.6)	1.5	101.3 (35.6)	42.5 (46.0)	5.0 (42.4)
GRLS-12-100	149.7 (8.3)	17.2	82.9 (4.5)	1.7	89.8 (83.4)	16.8 (43.7)	11.1 (22.0)

F_{max} = Maximum load, v_{max} = Displacement at the F_{max}, $F_{y,5\%}$ = Yield load by the 5% diameter method, $v_{y,5\%}$ = Displacement at the $F_{y,5\%}$, $k_{s,0.4}$ = Slip moduli $(0.4F_{exp.} - 0.1F_{exp.}/(v_{0.4,\,exp} - v_{0.1\,exp}))$, $k_{s,0.6}$ = Slip moduli $(0.6F_{exp.} - 0.1F_{exp.}/(v_{0.6,\,exp} - v_{0.1\,exp}))$, μ = Ductility index $(v_{max}/v_{y,5\%})$, ( )* = Coefficient of variation (%)

Table 5. Push-out Test Results for CLT-Steel Hybrid Connections

Specimens	Fastener type	Reinforcement	Dominant failure mode	Structural characteristics and descriptions
B-12-150	High-strength bolt (Ø12×150)	None	Mode III (two plastic hinges), Mode IV (bolt fracture)	High initial stiffness; high F_{max}; brittle post-peak response; moderate ductility
LS-10-125	Lag screw (Ø10×125)	None	Mode Ⅳ (screw fracture)	Lowest stiffness and strength; premature screw failures; high variability; limited ductility
LS-12-125	Lag screw (Ø12×125)	None	Mode Ⅲ + Ⅳ (Mixed)	Higher stiffness than LS-10-125; consistent load–slip response; wide plastic range; good ductility
LS-12-100	Lag screw (Ø12×100)	None	Mode Ⅲ + Ⅳ (Mixed)	Slightly lower F_{max} than LS-12-125; higher stiffness; stable post-peak softening; favorable ductility
CRLS-12-100	Lag screw (Ø12×100)	CFRP plate	Mode II (one plastic hinge), Mode IV (screw fracture)	Significantly increased stiffness and strength; suppressed timber bearing failure; brittle screw fracture; low ductility
GRLS-12-100	Lag screw (Ø12×100)	GF cloth	Mode III + IV (mixed)	Moderate stiffness and strength increase; partial suppression of timber failure; gradual softening; relatively favorable ductility

Reinforced lag screw connections

Specimen CRLS-12-100, reinforced with a CFRP plate (Fig. 5(e)), showed higher strength and stiffness than LS-12-100. The stiffness values ($k_{s,0.4}$ and $k_{s,0.6}$) increased by 75.9% and 254.2%, respectively, while the ultimate load (F_{max}) and yield load ($F_{y,5\%}$) increased by 37.7% and 77.3%, respectively. This improvement is attributed to the CFRP plate suppressing bearing failure in the CLT tensile lamina. However, the ductility index (μ = 5.0) was significantly lower, as the load capacity dropped abruptly after peak load without a noticeable softening region (COV: μ = 42.4%). In other words, CFRP reinforcement enhanced stiffness and strength substantially but promoted brittle screw fracture due to stress concentration.

Specimen GRLS-12-100, reinforced with GF cloth (Fig. 5(f)), showed moderate performance gains compared to LS-12-100, with $k_{s,0.4}$ and F_{max} increased by 55.9% and 13.9%, respectively. Although the strengthening effect was less pronounced than CFRP reinforcement, GRLS-12-100 exhibited a gradual increase in slip before reaching the ultimate load and maintained a softening response even after peak load (COV: μ = 22.0%). Thus, GF reinforcement produced a smaller increase in strength than CFRP reinforcement but maintained a more gradual post-peak response.

The results were compared with previous studies on lag-screw connections and GFRP-reinforced CLT joints. Rostampour Haftkhani *et al.* (2022) reported that GFRP reinforcement increased the lateral resistance of CLT double-shear joints by approximately 26.5%. In the present study, the GF cloth-reinforced specimen showed increases of 13.9% in maximum load and 55.9% in initial slip modulus compared with the unreinforced LS-12-100 specimen. The difference may be attributed to variations in joint configuration, reinforcement method, timber species, and fastener conditions. Abdoli *et al.* (2023) reported that fastener type and diameter affected the lateral resistance of CLT joints. Similarly, increasing the lag screw diameter from 10 to 12 mm at a constant length of 125 mm increased the maximum load from 61.2 to 153.7 kN. However, direct comparison is limited by differences in specimens, materials, and test conditions.

Analytical Load-Slip Model

The experimental load–slip curves show the joint behavior but do not provide parameters for numerical analysis. To characterize the average load–slip behavior of the CLT–steel hybrid joints in a quantitative manner, a nonlinear regression analysis was conducted using the Ramberg–Osgood model (Ramberg and Osgood 1943). This model was originally proposed to describe the stress–strain curves of metallic materials, but its application to timber–steel joints has been reported to capture complex nonlinear behavior (Hassanieh *et al.* 2016). The modified Ramberg–Osgood model proposed by Hassanieh *et al*. (2016) describes the initial elastic, post-yield, and softening stages using a single function (Eq. (1)). The model was fitted to the experimental load–slip curves,

$$F = \frac{(k_0 - k_p)\cdot s}{\left[1+\left(\frac{(k_0-k_p)\cdot s}{f_0}\right)^{n_1}\right]^{1/n_1}} + \frac{(k_p + k_s)\cdot s}{\left[1+\left(\frac{(k_p+k_s)\cdot s}{f_1 - f_0}\right)^{n_2}\right]^{1/n_2}} - k_s \cdot s \tag{1}$$

where F is the shear force, s is the slip, k_0 is the initial stiffness, k_p is the post-yield stiffness, k_s is the softening stiffness, f_0 is the shear force at the transition from the initial elastic to nonlinear region, f_1 is the shear force at the transition from post-yield to softening, and n_1 and n_2 are curvature parameters that control the sharpness of the first and second transitions, respectively. The model uses seven parameters, which can be related to the stiffness, strength, and post-yield response of the joints. For example, larger values of n_1 and n_2 make the curve transition sharper, indicating more brittle behavior. In addition, when k_s is less than zero, the load drops rapidly after reaching the maximum load.

Parameter estimation was carried out using a nonlinear least-squares method based on the Levenberg–Marquardt algorithm (Moré 2006), which was implemented with the *optimize.curve_fit* function of the Python SciPy package (Virtanen *et al.* 2020). From a total of 24 push-out tests, individual load–slip curves were obtained, and repeated optimization was carried out using the average load–slip curve of each joint. The goodness of fit was evaluated by the coefficient of determination (R^2), and all joints showed very high agreement with $R^2 > 0.99$.

The parameters summarized in Table 6 quantitatively describe the structural characteristics of each joint. The bolted joint (B-12-150) exhibited the highest initial stiffness (k_0 = 789.5 kN/mm), with k_s = −3.46 kN/mm capturing the abrupt post-peak degradation. The LS-10-125 specimen showed limited stiffness and strength due to its small screw diameter (k_0 = 104.9 kN/mm, f_1 = 73.9 kN). With increased diameter and length, LS-12-125 achieved higher strength (f_1 = 188.1 kN) and stability (n_2 = 10.0), enabling plateau formation after softening. LS-12-100, despite its relatively high stiffness (k_0 = 158.9 kN/mm), recorded a lower maximum load (f_1 = 164.4 kN) than LS-12-125, indicating the importance of embedment depth. For reinforced joints, CRLS-12-100 exhibited substantial improvements in stiffness and strength (k_0 = 612.5 kN/mm, f_1 = 156.2 kN), but with a steep softening slope (k_s = −2.81 kN/mm), consistent with the experimentally observed screw fractures. In contrast, GRLS-12-100 showed a lower stiffness increase (k_0 = 474.6 kN/mm) but a milder softening slope (k_s = −1.65 kN/mm), suggesting better load retention after peak and improved ductility compared to CFRP reinforcement.

Figure 6 visually confirms the strong agreement between the analytical and experimental results.

Table 6. Nonlinear Regression Parameters Obtained by Fitting the Modified Ramberg–Osgood Model Directly to the Mean Experimental Load–Slip Curve for Each CLT–Steel Hybrid Joint

Specimens	B-12-150	LS-10-125	LS-12-125	LS-12-100	CRLS-12-100	GRLS-12-100
Connector	Bolt	Lag screw	Lag screw	Lag screw	Lag screw	Lag screw
Reinforcement	None	None	None	None	CFRP plate	Glass fiber cloth
f_0 (kN)	21.3	27.2	95.7	90.0	7.2	22.5
f_1 (kN)	110.9	73.9	188.1	164.4	156.2	124.3
k_0 (kN/mm)	789.5	104.9	233.9	158.9	612.5	474.6
k_p (kN/mm)	32.95	13.59	3.49	2.81	107.4	54.6
k_s (kN/mm)	-3.46	0.236	1.25	1.59	-2.81	-1.65
n_1	3.933	2.006	0.804	1.116	8.594	2.555
n_2	3.005	3.391	10.0	10.0	2.826	1.427
R^2	0.9982	0.9938	0.9968	0.9966	0.9987	0.9941

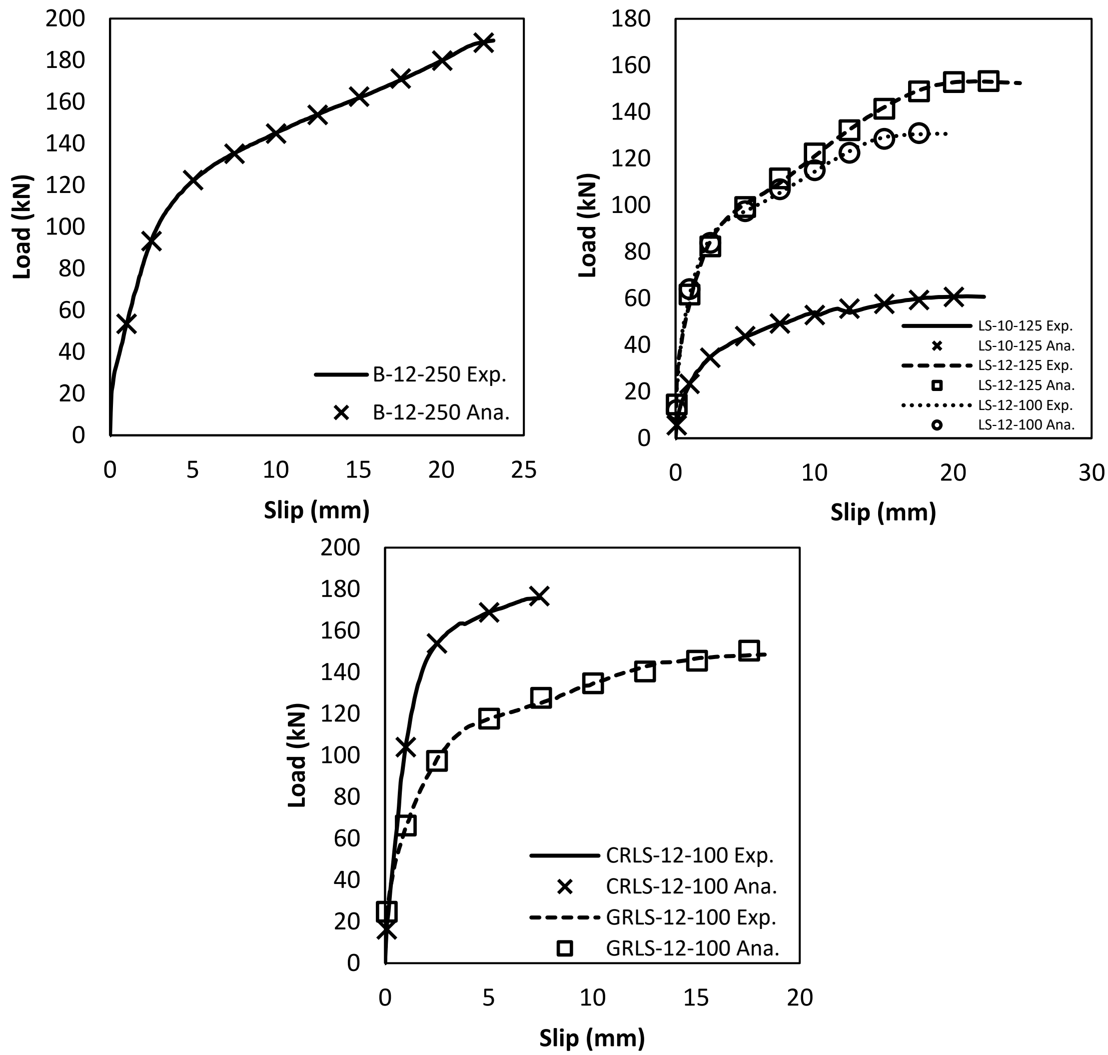

Fig. 6. Comparison of experimental and analytical load–slip curves for CLT–steel hybrid joints (B-12-150, LS-10-125, LS-12-125, LS-12-100, CRLS-12-100, GRLS-12-100)

The abrupt strength loss of the bolted joint, plateau formation in LS-12-125, premature drop in LS-12-100, sudden load degradation in CRLS-12-100, and gradual softening in GRLS-12-100 were consistently reproduced by the model. These results show that the Ramberg–Osgood model reproduced the measured load–slip behavior of the tested joints. Nevertheless, the model does not account for cyclic loading, fatigue, or long-term effects, which should be considered in future extensions. The parameters may be used as input data for nonlinear analysis after further validation.

CONCLUSIONS

1. The failure mechanisms of cross-laminated timber (CLT)–steel joints varied depending on the type of fastener, the length-to-diameter ratio (L/d), and reinforcement conditions. Bolted joints showed both Mode III plastic-hinge formation and Mode IV bolt fracture, while lag screw joints exhibited a mixture of Modes III and IV depending on diameter and embedment depth. Fiber-reinforced polymer (FRP) reinforcement effectively

suppressed timber damage; however, due to stiffness mismatch, carbon fiber-reinforced polymer (CFRP) tended to promote screw fractures, whereas glass fiber (GF) contributed to partial ductility improvement.

2. Bolted joints showed high stiffness and strength but experienced a sharp load decrease after the peak. The 12 mm lag screw joints exhibited stable softening and plateau behavior, and showed ductile behavior. Among the reinforced joints, CFRP plates significantly enhanced shear strength and stiffness but induced brittle failure through stress concentration, while GF cloth provided limited strength gains but contributed to ductility through gradual softening.
3. The Ramberg–Osgood-based model reproduced the load–slip curves of all joints with high accuracy ($R^2 > 0.99$). The model parameters (k_0, k_p, k_s, f_0, f_1, n_1, n_2) were related to the observed failure modes and ductility. Negative k_s values were associated with a rapid post-peak load decrease, whereas values close to zero indicated a more gradual post-peak response.
4. The experimental data obtained in this study (*e.g.*, F_{max}, F_y, k_s , μ) provide basic performance information for the design of CLT–steel joints, while the Ramberg–Osgood parameters may be used for nonlinear analysis after further validation. Among the tested systems, LS-12-125 showed relatively high strength and ductility without additional reinforcement. CFRP reinforcement increased strength and stiffness but caused brittle screw fracture, whereas GF reinforcement provided more gradual post-peak behavior. Further studies on cyclic loading, long-term behavior, full-scale floor systems, and cost are required before practical application.

ACKNOWLEDGEMENTS

This work was supported by the National Research Foundation of Korea (NRF) grant funded by the Korea government (MSIT) (No. 2022R1I1A3072085).

Conflict of Interest

The authors declare that they have no known competing financial interests or personal relationships that could have appeared to influence the work reported in this paper.

REFERENCES CITED

Abdoli, F., Rashidi, M., Rostampour-Haftkhani, A., Layeghi, M., and Ebrahimi, G. (2023). "Effects of fastener type, end distance, layer arrangement, and panel strength direction on lateral resistance of single shear lap joints in cross-laminated timber (CLT)," *Case Studies in Construction Materials* 18, article e01727. https://doi.org/10.1016/j.cscm.2022.e01727

Aloisio, A., Pasca, D. P., Owolabi, D., and Loss, C. (2024). "Vibration serviceability of hybrid CLT–steel composite floors based on experimental and numerical investigations using random walk models," *Engineering Structures* 304, article 117600. https://doi.org.10.1016/j.engstruct.2023.117600

Aspila, A., Heinisuo, M., Mela, K., Malaska, M., and Pajunen, S. (2022). "Elastic design of steel–timber composite beams," *Wood Material Science and Engineering* 17(4), 243-252. https://doi.org.10.1080/17480272.2021.1954799

Ataei, A., Valipour, H. R., Bradford, M. A., and Chiniforush, A. A. (2019). "Experimental study of steel–timber composite beam-to-column joints with extended end plates," *Construction and Building Materials* 226, 636-650. https://doi.org.10.1016/j.conbuildmat.2019.07.329

Azanaw, G. M. (2025). "Synergizing sustainability and structural innovation: A critical review of steel–CLT composite floor systems in modern construction," *Advances in Materials* 14(3), 80-87. https://doi.org.10.11648/j.am.20251403.14

Baek, S., Song, Y., and Hong, S. (2025). "Bending performance of domestic larch cross-laminated timber reinforced with fiber-reinforced polymer," *Wood Material Science and Engineering* 20(3), 686-696. https://doi.org.10.1080/17480272.2023.2276627

Bahrami, A., Vall, A., and Khalaf, A. (2021). "Comparison of cross-laminated timber and reinforced concrete floors with regard to load-bearing properties," *Civil Engineering and Architecture* 9(5), 1395-1408. https://doi.org.10.13189/cea.2021.090516

Brandner, R., Flatscher, G., Ringhofer, A., Schickhofer, G., and Thiel, A. (2016). "Cross laminated timber (CLT): Overview and development," *European Journal of Wood and Wood Products* 74(3), 331-351. https://doi.org.10.1007/s00107-015-0999-5

BS EN 26891 (1991). "Timber structures – Joints made with mechanical fasteners – General principles for the determination of strength and deformation characteristics," British Standards Institution, London, UK.

Chiniforush, A. A., Valipour, H. R., Bradford, M. A., and Akbarnezhad, A. (2019). "Long-term behaviour of steel–timber composite (STC) shear connections," *Engineering Structures* 196, article 109356. https://doi.org.10.1016/j.engstruct.2019.109356

Hassanieh, A., Valipour, H. R., and Bradford, M. A. (2016). "Load–slip behaviour of steel–cross laminated timber (CLT) composite connections," *Journal of Constructional Steel Research* 122, 110-121. https://doi.org.10.1016/j.jcsr.2016.03.019

Hassanieh, A., Valipour, H. R., and Bradford, M. A. (2017). "Experimental and numerical investigation of short-term behaviour of CLT–steel composite beams," *Engineering Structures* 144, 43-57. https://doi.org.10.1016/j.engstruct.2017.04.015

He, M., Zhang, Q., Sun, X., and Alhaddad, W. (2024). "An experimental and numerical study on the shear performance of friction-type high-strength bolted connections used for CLT–steel hybrid shear walls," *Engineering Structures* 306, article 117868. https://doi.org.10.1016/j.engstruct.2024.117868

Jung, H., Song, Y., and Hong, S. (2020). "Effect of glass fiber-reinforced connection on the horizontal shear strength of CLT walls," *Journal of the Korean Wood Science and Technology* 48(5), 685-695. https://doi.org.10.5658/WOOD.2020.48.5.685

KS F 2081 (2021). "Cross laminated timber," Korean Agency for Technology and Standards, Seoul, Korea.

KS D 3502 (2022). "Dimensions, mass and permissible variations of hot rolled steel sections," Korean Agency for Technology and Standards, Seoul, Korea.

Loss, C., and Frangi, A. (2017). "Experimental investigation on in-plane stiffness and strength of innovative steel–timber hybrid floor diaphragms," *Engineering Structures* 138, 229-244. https://doi.org.10.1016/j.engstruct.2017.01.064

Loss, C., Piazza, M., and Zandonini, R. (2016a). "Connections for steel–timber hybrid prefabricated buildings. Part I: Experimental tests," *Construction and Building Materials* 122, 781-795. https://doi.org/10.1016/j.conbuildmat.2016.06.099

Loss, C., Piazza, M., and Zandonini, R. (2016b). "Connections for steel–timber hybrid prefabricated buildings. Part II: Innovative modular structures," *Construction and Building Materials* 122, 796-808. https://doi.org/10.1016/j.conbuildmat.2016.06.098

Moré, J. J. (2006). "The Levenberg–Marquardt algorithm: Implementation and theory," in: *Numerical Analysis: Proceedings of the Biennial Conference Held at Dundee, June 28–July 1, 1977*, G. A. Watson (ed.), Springer, Berlin, pp. 105-116. https://doi.org/10.1007/BFb0067700

Moritani, F. Y., and Martins, C. E. (2021). "A literature review on cold-formed steel–timber composite structures," *BioResources* 16(4), 8489-8508. https://doi.org/10.15376/biores.16.4.8489-8508

Owolabi, D., and Loss, C. (2022). "Experimental and numerical study on the bending response of a prefabricated composite CLT–steel floor module," *Engineering Structures* 260, article 114278. https://doi.org/10.1016/j.engstruct.2022.114278

Ramage, M. H., Burridge, H., Busse-Wicher, M., Fereday, G., Reynolds, T., Shah, D. U., Wu, G., Li, Y., Fleming, P., Densley-Tingley, D., *et al*. (2017). "The wood from the trees: The use of timber in construction," *Renewable and Sustainable Energy Reviews* 68, 333-359. https://doi.org/10.1016/j.rser.2016.09.107

Ramberg, W., and Osgood, W. R. (1943). *Description of Stress–Strain Curves by Three Parameters* (No. NACA-TN-902), National Advisory Committee for Aeronautics Technical Note, Washington, DC.

Rostampour-Haftkhani, A., Abdoli, F., Hajializadeh, F., Rashidi, M., and Nasir, V. (2025). "Bending performance of cross-laminated timber reinforced with glass fibre-reinforced polymer and aluminium sheets," *International Wood Products Journal* 16(3), 213-224. https://doi.org/10.1177/20426445251362979

Rostampour Haftkhani, A., Rashidi, M., Abdoli, F., and Gerami, M. (2022). "The effect of GFRP wrapping on lateral performance of double shear lap joints in cross-laminated timber as a part of timber bridges," *Buildings* 12(10), article 1678. https://doi.org/10.3390/buildings12101678

Song, Y. J., and Hong, S. I. (2018). "Performance evaluation of the bending strength of larch cross-laminated timber," *Wood Research* 63(1), 105-116.

Song, Y. J., Baek, S. Y., Kim, H. W., and Hong, S. I. (2024). "Behavior of laminated timber portal frames reinforced with fiber-reinforced plastic laminates under cyclic lateral load," *BioResources* 19(4), 9132-9147. https://doi.org/10.15376/biores.19.4.9132-9147

Song, Y. J., Baek, S. Y., Yu, S. H., Kim, D. H., and Hong, S. I. (2022). "Evaluation of the bending performance of glued CLT–concrete composite floors based on the CFRP reinforcement ratio," *BioResources* 17(2), 2243-2259. https://doi.org/10.15376/biores.17.2.2243-2259

Song, Y. J., Lee, I. H., and Hong, S. I. (2019a). "An evaluation of strength performance of the edge connections between cross-laminated timber panels reinforced with glass fiber-reinforced plastic," *BioResources* 14(4), 7719-7733. https://doi.org/10.15376/biores.14.4.7719-7733

Song, Y. J., Lee, I. H., and Hong, S. I. (2019b). "Evaluation of horizontal shear performance of larch CLT walls according to the edge connection shape," *Wood Research* 64(2), 213-222.

Vahedian, A., Shrestha, R., and Crews, K. (2019). "Experimental and analytical investigation on CFRP strengthened glulam laminated timber beams: Full-scale experiments," *Composites Part B: Engineering* 164, 377-389. https://doi.org.10.1016/j.compositesb.2018.11.049

Virtanen, P., Gommers, R., Oliphant, T. E., Haberland, M., Reddy, T., Cournapeau, D., Burovski, E., Peterson, P., Weckesser, W., Bright, J., *et al*. (2020). "SciPy 1.0: Fundamental algorithms for scientific computing in Python," *Nature Methods* 17(3), 261-272. https://doi.org.10.1038/s41592-019-0686-2

Yang, H., Wu, Y., Shi, B., Tao, H., and Huang, H. (2025). "Performance of Deltabeam–CLT composite floors under human-induced vibration," *Buildings* 15(12), article 2074. https://doi.org.10.3390/buildings15122074

Yin, X. (2018). "The seismic behavior of cross-laminated-timber composite slab in high-rise building," *International Journal of Engineering and Technology* 10, 325-328. https://doi.org.10.7763/IJET.2018.V10.1065

Younis, A., and Dodoo, A. (2022). "Cross-laminated timber for building construction: A life-cycle-assessment overview," *Journal of Building Engineering* 52, article 104482. https://doi.org.10.1016/j.jobe.2022.104482

Zhang, H., and Ling, Z. (2022). "Finite element modeling on shear performance of grouted stud connectors for steel–timber composite beams," *Materials* 15(3), article 1196. https://doi.org.10.3390/ma15031196

Article submitted: September 23, 2025; Peer review completed: November 15, 2026; Revised version received and accepted: September 6, 2026; Published: September 18, 2026.
DOI: 10.15376/biores.21.4.10835-10852